Article

Current Biology

MpFEW RHIZOIDS1 miRNA-Mediated Lateral Inhibition Controls Rhizoid Cell Patterning in *Marchantia polymorpha*

Graphical Abstract

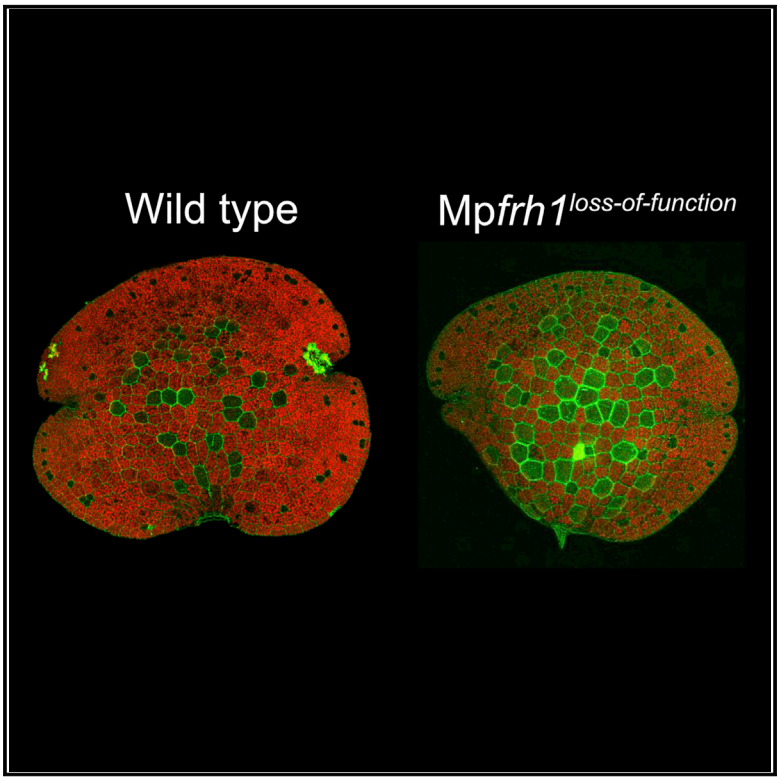

Authors

Anna Thamm, Timothy E. Saunders, Liam Dolan

Correspondence

liam.dolan@plants.ox.ac.uk

In Brief

Lateral inhibition patterns cells during the development of multicellular organisms. Thamm et al. show that lateral inhibition patterns rhizoid cells in the *Marchantia polymorpha* epidermis using a combination of modeling and genetics. MpFRH1 miRNA provides the repressor activity in this new molecular mechanism of lateral inhibition.

Highlights

- Lateral inhibition produces the pattern of rhizoid cells in *Marchantia polymorpha*
- Modeling predicts a rhizoid cell pattern that would develop without lateral inhibition
- Mp*frh1* mutants develop a rhizoid cell pattern as predicted without lateral inhibition
- MpFRH1 (repressor) inhibits MpRSL1 (activator) in patterning by lateral inhibition

Thamm et al., 2020, Current Biology *30*, 1905–1915
May 18, 2020
https://doi.org/10.1016/j.cub.2020.03.032

CellPress

Current Biology
Article

CellPress

MpFEW RHIZOIDS1 miRNA-Mediated Lateral Inhibition Controls Rhizoid Cell Patterning in *Marchantia polymorpha*

Anna Thamm,[1] Timothy E. Saunders,[2] and Liam Dolan[1,3,*]
[1]Department of Plant Sciences, University of Oxford, Oxford OX1 3RB, UK
[2]Mechanobiology Institute and Department of Biological Sciences, National University of Singapore, 117411 Singapore, Singapore
[3]Lead Contact
*Correspondence: liam.dolan@plants.ox.ac.uk
https://doi.org/10.1016/j.cub.2020.03.032

SUMMARY

Lateral inhibition patterns differentiated cell types among equivalent cells during development in bacteria, metazoans, and plants. Tip-growing rhizoid cells develop among flat epidermal cells in the epidermis of the early-diverging land plant *Marchantia polymorpha*. We show that the majority of rhizoid cells develop individually, but some develop in linear, one-dimensional groups (chains) of between 2 and 7 rhizoid cells in wild-type plants. The distribution of rhizoid cells can be accounted for within a simple cellular automata model of lateral inhibition. The model predicted that in the absence of lateral inhibition, two-dimensional rhizoid cell groups (clusters) form. These can be larger than those formed with lateral inhibition. *M. polymorpha* rhizoid differentiation is positively regulated by the ROOT HAIR DEFECTIVE SIX-LIKE1 (MpRSL1) basic-helix-loop-helix (bHLH) transcription factor, which is directly repressed by the FEW RHIZOIDS1 (MpFRH1) microRNA (miRNA). To test if MpFRH1 miRNA acts during lateral inhibition, we generated loss-of-function (lof) mutants without the MpFRH1 miRNA. Two-dimensional clusters of rhizoids develop in Mp*frh1*^{lof} mutants as predicted by the model for plants that lack lateral inhibition. Furthermore, two-dimensional clusters of up to 9 rhizoid cells developed in the Mp*frh1*^{lof} mutants compared to a maximum number of 7 observed in wild-type groups. The higher steady-state levels of Mp*RSL1* mRNA in Mp*frh1*^{lof} mutants indicate that MpFRH1-mediated lateral inhibition involves the repression of MpRSL1 activity. Together, the modeling and genetic data indicate that MpFRH1 miRNA mediates lateral inhibition by repressing MpRSL1 during pattern formation in the *M. polymorpha* epidermis.

INTRODUCTION

Spatial arrays of diverse cell types develop from populations of equivalent cells during the development of multicellular organisms. The patterning of these different cell types involves lateral inhibition, a process in which an individual cell instructs adjacent cells to acquire an identity that is different from the fate of the instructing cell. In metazoans, lateral inhibition involves cell-to-cell signaling carried out by the Delta-Notch ligand-receptor pair (reviewed in [1–3]). Neither Delta nor Notch proteins are present in plants, and other mechanisms of lateral inhibition operate in the angiosperm *Arabidopsis thaliana* [4–6]. Computational modeling suggests that the production of EPIDERMAL PATTERNING FACTOR2 (EPF2) peptide by meristemoids inhibits meristemoid development in adjacent cells during guard cell development in leaves [7–9]. The cell-to-cell movement of Myb transcriptional repressor proteins pattern trichomes (leaf hair cells) among pavement epidermal cells in the *A. thaliana* shoot epidermis [10]. Therefore, lateral inhibition mechanisms exist in plants where proteins move from one cell to another to modulate the development of the receiving cell.

Rhizoid cells develop from fields of equivalent cells in the epidermis of the liverwort *Marchantia polymorpha*, an early-diverging land plant. Flat epidermal cells occupy the space between rhizoid cells. The ROOT HAIR DEFECTIVE SIX-LIKE1 (RSL1) basic-helix-loop-helix transcription factor is necessary and sufficient for rhizoid cell development [11–13]. Rhizoid cells do not develop in plants harboring loss-of-function mutations in Mp*RSL1* (Mp*rsl1*^{lof}), and flat epidermal cells develop in their place [13]. Conversely, plants harboring Mp*RSL1* gain-of-function mutations develop supernumerary, ectopic rhizoids in place of flat epidermal cells [13]. MpRSL1 promotes the expression of Mp*FEW RHIZOIDS1* (Mp*FRH1*), which encodes a 21-nt microRNA (miRNA) [14]. Evidence that MpFRH1 represses rhizoid cell development by negatively regulating MpRSL1 activity includes the observations that (1) MpFRH1 miRNA directly targets RSL1 mRNA for cleavage and (2) the rhizoidless phenotype of Mp*FRH1* overexpression is suppressed by co-expressing an MpFRH1 miRNA-resistant version of MpRSL1 [14]. Therefore, MpRSL1 and MpFRH1 act together in a network with negative feedback in which the transcription factor is an activator of rhizoid cell development and the miRNA is a repressor of rhizoid cell development.

Since MpRSL1 and MpFRH1 constitute an activator-repressor network with negative feedback, we hypothesized that the MpFRH1 miRNA could be involved in lateral inhibition during the patterning of rhizoid cells in the epidermis *M. polymorpha* [14]. To test this hypothesis, we first utilized a simple cellular

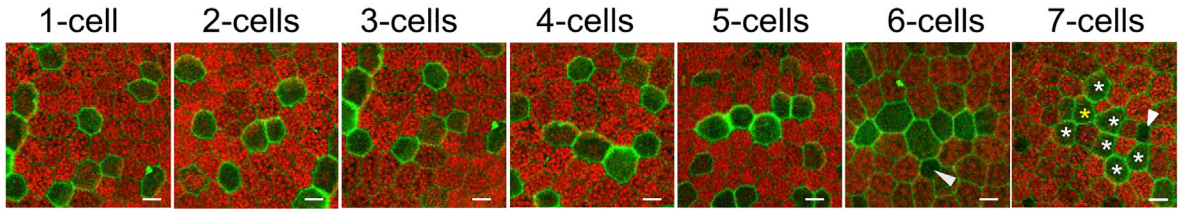

Tak-1	72.8 %	18.5 %	4.3 %	3.1 %	0.8 %	0.4 %	0.4 %
Tak-2	69.1 %	18.8 %	7.3 %	2.6 %	1 %	1 %	-
Mean RCN	0 ± 0	1 ± 0	1.36 ± 0.13	1.57 ± 0.27	1.6 ± 0	1.67 ± 0	1.71 ± NA

Figure 1. Organization of Rhizoid Cell Groups in the Wild-Type *M. polymorpha* Gemma Epidermis

Representative examples of individual rhizoid cells and rhizoid cell groups of between 2 and 7 rhizoid cells on mature gemmae of Tak-1 and Tak-2 wild-type accessions. Rhizoid groups are generally arranged in one-dimensional, linear arrays that we call chains. Rhizoid cells in chains develop 2 rhizoid cell neighbors, except when they are located at the end of the chain, where they develop only 1 rhizoid cell neighbor. Exceptionally, two-dimensional clusters were observed, as indicated in the 7-cell rhizoid group shown here, where a single cell developed 3 rhizoid cell neighbors (yellow asterisk). Images of 1-cell, 3-cell, and 4-cell rhizoid cell groups are from the same gemma. Chlorophyll autofluorescence is red, and cell walls of rhizoid cells are stained with propidium iodide (green). Tabular presentation of the frequencies of each rhizoid cell group size class. The values represent the frequency of rhizoid cell groups of each class as a percentage of the total number of rhizoid cell groups. The mean rhizoid cell neighbor number (RCN) for each size class is presented ± SD (n [Tak-1] = 22 gemmae, n [Tak-2] = 23). Scale bar, 20 μm; arrowheads indicate the position of oil body cells, which are distinguished from rhizoid cells because of their smaller size and shape. The asterisks in the 7-cell rhizoid group indicate rhizoid cells. An image of the gemma on which the 7-rhizoid cell cluster developed is shown in Figure S1.

automata model to simulate the effects of lateral inhibition on the pattern of rhizoid cell spacing based on wild-type conditions (full model details are in the Results and STAR Methods). This revealed that the spatial distribution of rhizoid cells in wild type was consistent with lateral inhibition being involved in patterning. We then ran the model in the absence of lateral inhibition to predict the rhizoid cell distribution that would be observed in a plant in which lateral inhibition did not operate. To test if MpFRH1 miRNA was involved in lateral inhibition, we characterized rhizoid cell distribution in Mp*frh1*^{lof} mutants. The distribution of rhizoid cells in Mp*frh1*^{lof} mutants was consistent with the predicted distribution from the model without lateral inhibition. These data indicate that MpFRH1 miRNA acts in the lateral inhibition of rhizoid cell development during epidermal development in *M. polymorpha.*

RESULTS

One-Dimensional Groups (Chains) of Rhizoid Cells Developed in Wild-Type *M. polymorpha* Gemma Epidermis

The *M. polymorpha* gemma epidermis comprises flat epidermal cells that surround rhizoid cells. Rhizoid cells produce a tip-growing projection that penetrates the growth substrate and carries out rooting function. To determine if lateral inhibition is involved in the patterning of rhizoid cells among flat epidermal cells, we characterized the spatial arrangement of rhizoid cells in the epidermis of wild-type gemmae (Tak-1 and Tak-2). Rhizoid cells developed individually and in groups in wild type (Figure 1; Table 1). The majority (~70%) developed individually, surrounded by flat epidermal cells. In the Tak-2 wild-type background, ~30% of rhizoids developed as groups of between 2 and 6 rhizoid cells (Table 1); 18.8% 7.3%, 2.6%, 1.0%, and 1.0% of rhizoids formed in groups of 2, 3, 4, 5, and 6 rhizoid cells, respectively. Most rhizoid cell groups were arranged in a one-dimensional linear array, like beads on a string, that we designate a chain. Rhizoid cells at either end contacted 1 neighboring rhizoid cell, while internal rhizoid cells contacted 2 rhizoid cells. Consequently, in a one-dimensional group of 3 rhizoid cells, there were 2 rhizoid cells on either end of the chain with a single rhizoid cell between each of these end initials. Therefore, such a chain of 3 develops an average of 1.33 rhizoid cell neighbors ((1 + 2 + 1)/3 = 1.33). The rhizoid cells in 24 of the 25 3-rhizoid cell groups were arranged as one-dimensional chains. Rhizoids were not arranged in a string in one 3-rhizoid cell group. Each of the adjacent rhizoid cells in this single 3-rhizoid cell group had an average of 2 rhizoid cell neighbors, making the group two-dimensional. We designate such a 2-dimensional arrangement of rhizoid cells a cluster. The average number of rhizoid cell neighbors in 3-rhizoid cell groups was 1.36 (SD = 0.13; n = 25). The mean number of rhizoid cell neighbors increases as group size increases in wild type. For example, in a one-dimensional group of 4 rhizoid cells, there was an average of 1.5 rhizoid cell neighbors ((1 + 2 + 2 + 1)/4 = 1.5). Rhizoid cells in 12 of 13 4-rhizoid cell groups were arranged as one-dimensional chains, while there was a single case of a two-dimensional cluster. Therefore, the mean rhizoid cell neighbor number in 4-cell groups is 1.57 (SD = 0.27; n = 13). We observed four 5-rhizoid cell groups and three 6-cell rhizoid groups, and rhizoid cells were arranged as one-dimensional chains in each group. Therefore, the average rhizoid cell neighbor number was 1.60 in 5-cell groups (SD = 0; n = 4) and 1.66 in 6-cell groups (SD = 0; n = 3) (Figure 1). There was a single, two-dimensional, 7-cell cluster in the Tak-1 background (Figures 1 and S1).

For one-dimensional rhizoid arrays with n cells, the average rhizoid cell neighbor number is 2(n − 1)/n. The SD is close to zero, indicating that this pattern is consistent for each rhizoid cell group size. In total, 93.5% of wild-type rhizoid cell groups

Table 1. Frequency of Individual Rhizoid Cells and Rhizoid Groups in Wild Type and Mp*frh1*^{lof} and Mp*RSL1*^{GOF} Mutants

Genotype	1	2	3	4	5	6	7	8	9	≥10	Cluster (n)	Gemmae (n)
Tak-1	72.5%	18.4%	4.3%	3.1%	0.8%	0.4%	0.4%				255	22
Tak-2	69.1%	18.8%	7.3%	2.6%	1.0%	1.0%					191	23
Mp*frh1*$^{lof-7}$	47.1%	23.2%	12.3%	9.0%	4.5%	1.3%		0.6%	1.9%		155	42
Mp*frh1*$^{lof-11}$	61.4%	23.8%	7.4%	4.8%	1.6%	0.5%	0.5%				189	27
Mp*frh1*$^{lof-27}$	63.2%	23.0%	9.8%	0.6%	1.1%	1.1%	0.6%	0.6%			174	22
Mp*frh1*$^{lof-34}$	48.0%	40.0%	8.0%	4.0%							75	9
Mp*frh1*$^{lof-36}$	69.4%	19.4%	6.9%	1.4%	2.8%						72	8
Mp*RSL1*$^{GOF-1}$	58.6%	14.1%	13.1%	5.1%	3.0%	1.0%	2.0%			3.0%	99	10

are arranged in one-dimensional chains, and only 6.5% are arranged in two-dimensional clusters (n = 46). The typical maximum number of rhizoid cell neighbors is 2, because groups comprise one-dimensional linear arrays of rhizoid cells. This is consistent with the hypothesis that lateral inhibition operates in the patterning of rhizoid cells in the epidermis.

Modeling Predicts that Lateral Inhibition Is Involved in the Distribution of Rhizoid Cells in Wild-Type Gemma Epidermis

A simple cellular automata model for the development of rhizoid cells among flat epidermal cells in the gemma epidermis was developed to test if lateral inhibition might be involved in epidermal pattern formation [15, 16]. Such modeling approaches are a powerful method for dissecting biological processes, such as tumor growth and cell sorting [17, 18]. We initiated a hexagonal lattice of cells with seeds for individual and separated rhizoid cells at a density similar to that measured experimentally (complete details are presented in STAR Methods), meaning that at the start of each simulation run, the largest group of rhizoid cells had a size of 1. The lattice had hard-wall boundary conditions. Such boundary conditions restrict the size of rhizoid clusters near the system edge but more accurately reflect the spatial constraints on the developing tissue. In the following runs of the simulation, additional rhizoid cells developed by satisfying two rules. According to rule 1, for each group of rhizoid cells, at each simulation step, a probability P determined whether a new neighboring cell becomes part of the rhizoid group or $(1 - P)$ whether the group stops adding new rhizoid cells (and stays fixed at that rhizoid cell number for remainder of simulation, i.e., inactive). A unique generated uniform random number between 0 and 1 was used to test this rule for each active group of rhizoid cells during each iteration of the simulation. To incorporate new rhizoid cells into a pre-existing group in wild-type conditions, we then applied rule 2, where the new rhizoid cell had to be a neighbor to precisely 1 existing rhizoid cell (no fewer and no more) (Figure 2A, top). The new rhizoid cell was selected randomly from the neighboring cells that obeyed the lateral inhibition rule. The simulation ceased when all rhizoid groups became inactive. No other rules were incorporated into the model. We ran 1,000 simulations for each condition, and the results shown are for the average neighbor number across all simulations (Figure 2). See Figure S2 for examples of the simulation output during different stages of the simulation.

The only parameter, P = 0.33, was fixed by matching the simulation to the observed distribution of wild-type rhizoid cell group sizes (Figure 2B). The simulated rhizoid cell groups were always one-dimensional chains (i.e., linear) when lateral inhibition was present (Figure 2C). The model replicated the observed wild-type distributions of rhizoid cell neighbor frequency (Figure 2D), with near zero SD because cell groups were almost always one-dimensional chains (Figure 2C). Thus, simple lateral inhibition is consistent with our observed patterns of rhizoid cell development and also with the invariant neighbor number.

We next considered the scenario whereby rule 2 was relaxed so that a new rhizoid cell can develop next to one or more existing rhizoid cells; i.e., we remove the lateral inhibition requirement (Figure 2A, bottom). Once a rhizoid group is selected for expansion, any neighboring cell is randomly chosen to add to the group. The resulting pattern did not resemble the pattern of rhizoid cells in wild-type plants (Figure 2E), because the frequency of two-dimensional clusters markedly increased. Because of the increased frequency of these two-dimensional clusters, the mean and variability (SD) in the number of rhizoid cell neighbors was greater than when the model operated with lateral inhibition (Figure 2F).

Using our given P, groups of 7 or more cells are extremely rare in the wild-type simulations (0.1% of rhizoid cell groups) where lateral inhibition is active, which is consistent with what is observed in wild-type plants (where groups of more than 7 cells were not observed). However, in our simulations with the relaxed rule 2, groups can merge; in the absence of lateral inhibition, two groups of rhizoid cells are not inhibited from adding a linking rhizoid cell between them. In this case, larger two-dimensional clusters form, with a maximum cluster size of 12 cells observed in the model (Figure S2). Such mergers increase the mean and SD of the rhizoid cell neighbor number. Furthermore, these clusters are rounder than the elongated, one-dimensional chains that develop in wild type (Figure 2E).

These modeling results indicate that if lateral inhibition controls the spacing of rhizoid cells in *M. polymorpha*, then loss of this mechanism will cause development of two-dimensional rhizoid cell clusters, including occasional very large clusters. We emphasize that these quantitative model predictions require no extra parameters; they are simply dependent on the presence/absence of lateral inhibition (rule 2). Of course, other more complex (and realistic) models can be considered, for example by including dynamics more explicitly. However, our simple Boolean-like lateral inhibition model is consistent with the hypothesis that lateral inhibition functions during the patterning of rhizoid cells; a rhizoid cell can develop next to flat epidermal cells or a single rhizoid but never more than one

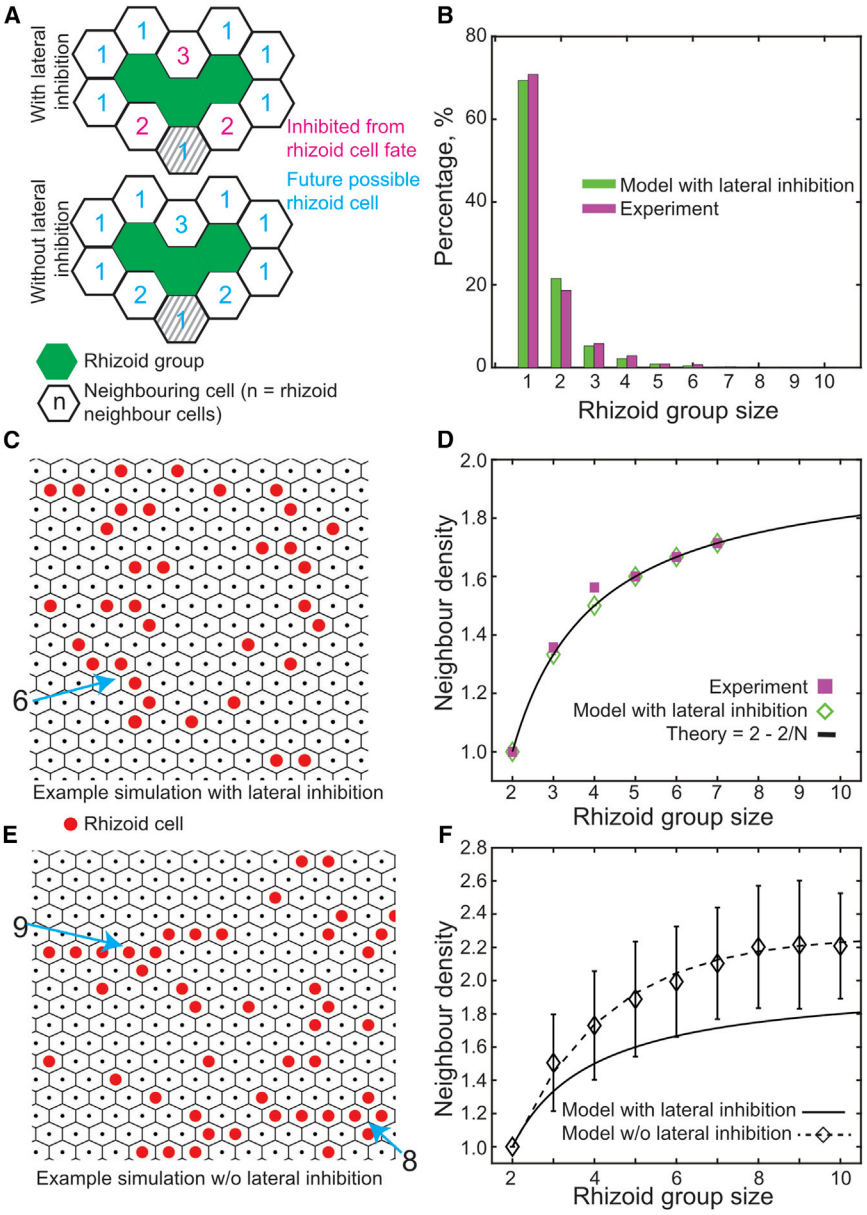

Figure 2. Cellular Automata Modeling Indicates that Lateral Inhibition Can Account for the Patterning of Rhizoid Cells in the *M. polymorpha* Gemma

(A) Schematic of lateral inhibition model of rhizoid development. Top: lateral inhibition restricts the addition of a new cell to a rhizoid group to those only neighboring a single rhizoid cell. Bottom: in the absence of lateral inhibition, any cell can differentiate as a rhizoid cell. The gray cell represents a new possible rhizoid cell that has a single rhizoid neighbor yet is not adjacent to the end of the rhizoid cluster. We exclude such a possibility in the simulations for wild type, but including this does not alter the statistical results.

(B) Validation of lateral inhibition model by comparing the frequency distribution of rhizoid cell group size produced by the model (green, n = 1,000 simulations) and those observed in wild-type gemma epidermis (magenta, "experiment," n = 45 gemmae).

(C) Output of the lateral inhibition model showing rhizoid cell distribution (red) and flat epidermal cells (white) in the gemma epidermis. In the presence of lateral inhibition, each rhizoid group forms a one-dimensional chain. A group of 6 rhizoid cells is highlighted.

(D) Validation of lateral inhibition model by comparing the relationship between mean rhizoid cell neighbor number and rhizoid cluster size as predicted by the model (green) with data from wild-type gemmae (magenta).

(E) Output of the model without lateral inhibition, showing the distribution of rhizoid cells (red) and flat epidermal cells (white) in the gemma epidermis. In the absence of lateral inhibition, rhizoid groups can develop into two-dimensional clusters. Groups of 8 and 9 rhizoid cells are highlighted.

(F) Predicted relationship between mean rhizoid cell neighbor number and rhizoid group size in the presence and absence of lateral inhibition. The solid black line represents the output from the model that includes lateral inhibition. The diamonds (error bars represent ± 1 SD, n = 1,000 simulations) represent the output of the model without lateral inhibition, with the dashed line representing a best fit to $1 + 1.27[1 - \exp(-((N-2)/2.3))]$. The mean rhizoid cell neighbor number and the variability in neighbor number is greater in the absence of lateral inhibition. Selected individual steps in the simulation are shown in Figure S2.

rhizoid cell. The model also provides quantitative predictions for the variability in cluster size and connectivity in mutants with defective lateral inhibition.

Two-Dimensional Groups of Rhizoid Cells (Clusters) Developed in Mp*frh1* Mutants

If MpFRH1 miRNA mediates lateral inhibition during rhizoid cell development, then the model predicted that two-dimensional rhizoid groups of rhizoid cells (clusters) would develop in Mp*frh1*^{lof} mutants while one-dimensional groups of rhizoid cells (chains) would develop in wild type. To determine if MpFRH1 miRNA is involved in lateral inhibition, we generated mutants in which the entire Mp*FRH1* miRNA coding sequence was deleted. We used a pair of single guide RNAs (sgRNAs) that were 569 bp apart to delete the MpFRH1 gene using CRISPR/Cas9 technology [19]. sgRNA1 was 20 bp long and was complementary to a sequence between 404 bp and 384 bp 5′ of the Mp*FRH1* miRNA sequence (sgRNA1), and sgRNA2 was 20 bp long and complementary to a sequence between 164 bp and 184 bp 3′ of the Mp*FRH1* miRNA sequence (Figure 3A). Five independent mutant lines were identified in which the entire Mp*FRH1* miRNA sequence was deleted. There were deletions of 267, 587, 589, and 573 bp in the Mp*FRH1* gene of Mp*frh1*-7, Mp*frh1*-27, Mp*frh1*-34, and Mp*frh1*-36 mutants, respectively. In Mp*frh1*-11, a 780-bp deletion, removed the Mp*FRH1* sequence, and a 202-bp sequence inserted 5′ of the Mp*FRH1* sequence (Figure 3A; Data S1). Mp*FRH1* miRNA was not detected (Figure 3B) in any of the five deletion mutants consistent with the hypothesis

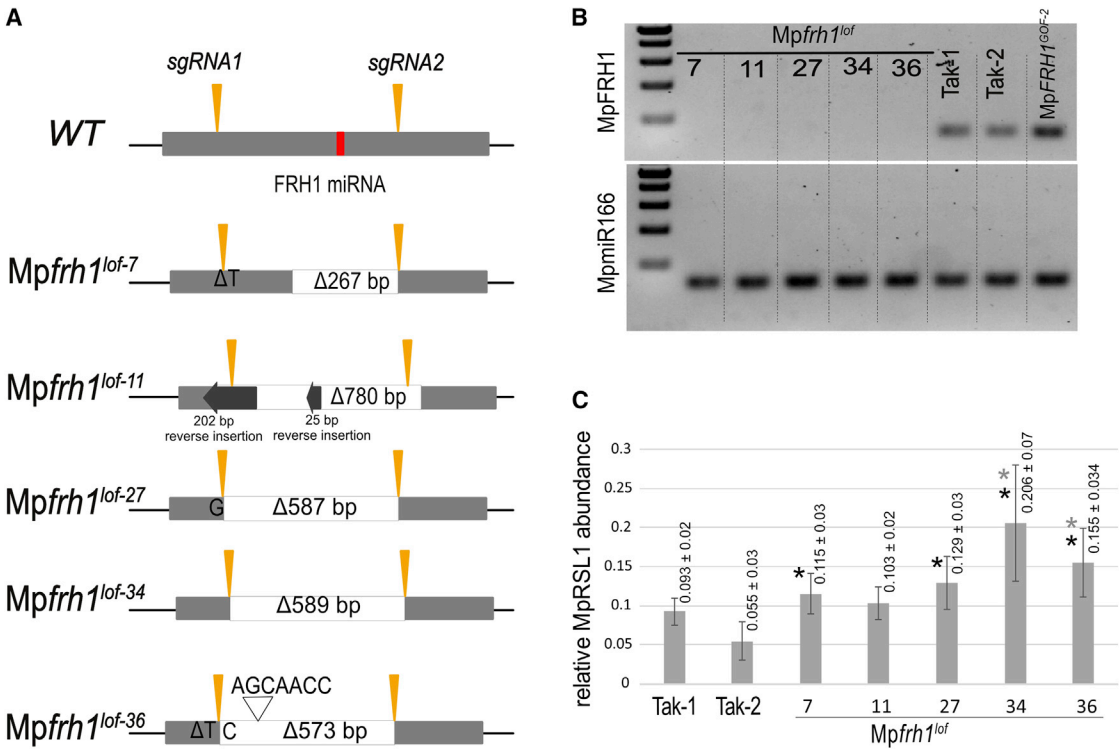

Figure 3. Genomic Organization of Mp*frh1*^{lof} Mutants and Expression of Mp*RSL1* and Mp*FRH1* in Mp*frh1*^{lof} Mutants

(A) Genomic organization of the Mp*FRH1* gene in wild type (WT) and Mp*frh1*^{lof} mutants. The sequence for the 1.2-kb Mp*FRH1* transcript is represented with a gray box. The 21 nt corresponding to the Mp*FRH1* miRNA are indicated in red. The orange arrowheads indicate the position of the two single guide RNAs (sgRNAs) used to generate deletion mutants. sgRNA1 is complementary to a sequence that is between 384 and 404 bp 5′ of the Mp*FRH1* sequence. sgRNA2 is complementary to a sequence that is 164–184 3′ of the Mp*FRH1* sequence. The entire Mp*FRH1* miRNA sequence was deleted in each of the mutants. In Mp*frh1*$^{lof-7}$, there was a 267-bp deletion between sgRNA1 and sgRNA2 and a T deletion. In Mp*frh1*$^{lof-11}$, there was a deletion of 780 bp and reverse insertions of 202 bp and 26 bp. In Mp*frh1* $^{lof-27}$, there was a 587-bp deletion and a G insertion. In Mp*frh1*$^{lof-34}$, there was a 589-bp deletion. In Mp*frh1*$^{lof-36}$, there was a 573-bp deletion and substitution of T into C at the sgRNA1 target site and a 7 bp insertion.

(B) Amplification of MpFRH1 miRNA (upper row) and MpmiR166 control (lower row) using stem loop PCR on RNA isolated from 7-day-old thalli grown from gemmae in Mp*frh1*^{lof} mutants, Tak-1, Tak-2, and Mp*FRH1*$^{GOF-2}$ mutant.

(C) Amplification of Mp*RSL1* mRNA from RNA isolated from in 7-day-old thalli grown from gemmae in wild-type (Tak-1 and Tak-2) plants and Mp*frh1*^{lof} mutants; mRNA levels were normalized to the housekeeping gene Mp*APT1*. There were three biological replicates per genotype, except for Mp*frh1*$^{lof-7}$(n = 2). There were at least three technical replicates per biological replicate. Error bars represent ± SD. A gray asterisk indicates a significant difference compared with Tak-1, and a black asterisk indicates a significant difference compared with Tak-2. $p < 0.05$.

Results for independent verification of qPCR results are presented in Figure S3.

that each harbored complete loss-of-function mutations in Mp*FRH1*. Consequently, the mutants were designated Mp*frh1*$^{lof-7}$, Mp*frh1*$^{lof-11}$, Mp*frh1*$^{lof-27}$, Mp*frh1*$^{lof-34}$, and Mp*frh1*$^{lof-36}$.

To determine if the pattern of rhizoids in Mp*frh1*^{lof} mutants was as predicted by the model in the absence of lateral inhibition, the number of rhizoid cell neighbors was measured in rhizoid cell groups in each of the mutants. The model predicted that the number of rhizoid cell neighbors in the absence of lateral inhibitions would be greater than in wild type. As predicted by the model, the mean rhizoid cell neighbor number was greater in the Mp*frh1*^{lof} mutants than in wild type (Figures 4B and 5). In all five Mp*frh1*^{lof} mutants, the mean number of neighbors in groups of 3 rhizoid cells was greater than the corresponding neighbor number in wild type (e.g., 1.36, SD = 0.13). Furthermore, while the SD was close to 0 in wild type, indicating that there was little variation in the mean number of neighbor cells per rhizoid group, the SD was always greater than 0 in the mutants. For example, there were on average 1.40 (SD = 0.21) rhizoid cell neighbors in groups of 3-rhizoid cells in Mp*frh1*$^{lof-7}$, 1.45 (SD = 0.26) rhizoid cell neighbors in Mp*frh1*$^{lof-27}$, 1.48 (SD = 0.28) rhizoid cell neighbors in Mp*frh1*$^{lof-11}$, 1.56 (SD = 0.34) in Mp*frh1*$^{lof-34}$ and 1.60 (SD = 0.37) in Mp*frh1*$^{lof-36}$ (Figures 5A and 5E). The same trend held for groups of 4 rhizoid cells, where the number of rhizoid cell neighbors was 1.57 (SD = 0.27) in wild type (1.63 for Tak-1 [SD = 0.35] and 1.5 in Tak-2 [SD = 0]). Groups containing 4 rhizoid cells developed an average of 1.73 (SD = 0.37) rhizoid cell neighbors in Mp*frh1*$^{lof-7}$, 1.61 (SD = 0.33) in Mp*frh1*$^{lof-11}$, and 1.67 (SD = 0.29) in Mp*frh1*$^{lof-34}$ mutants (Figures 5B and 5E). Groups of 5 rhizoid cells in Mp*frh1*$^{lof-27}$ developed 2.20 (SD = 0.28) rhizoid cell neighbors compared to 1.60 (SD = 0) in wild type (Figures 5C and 5E). We conclude that rhizoid cell clusters groups are frequently arranged in two-dimensional clusters in Mp*frh1*^{lof} mutants rather than

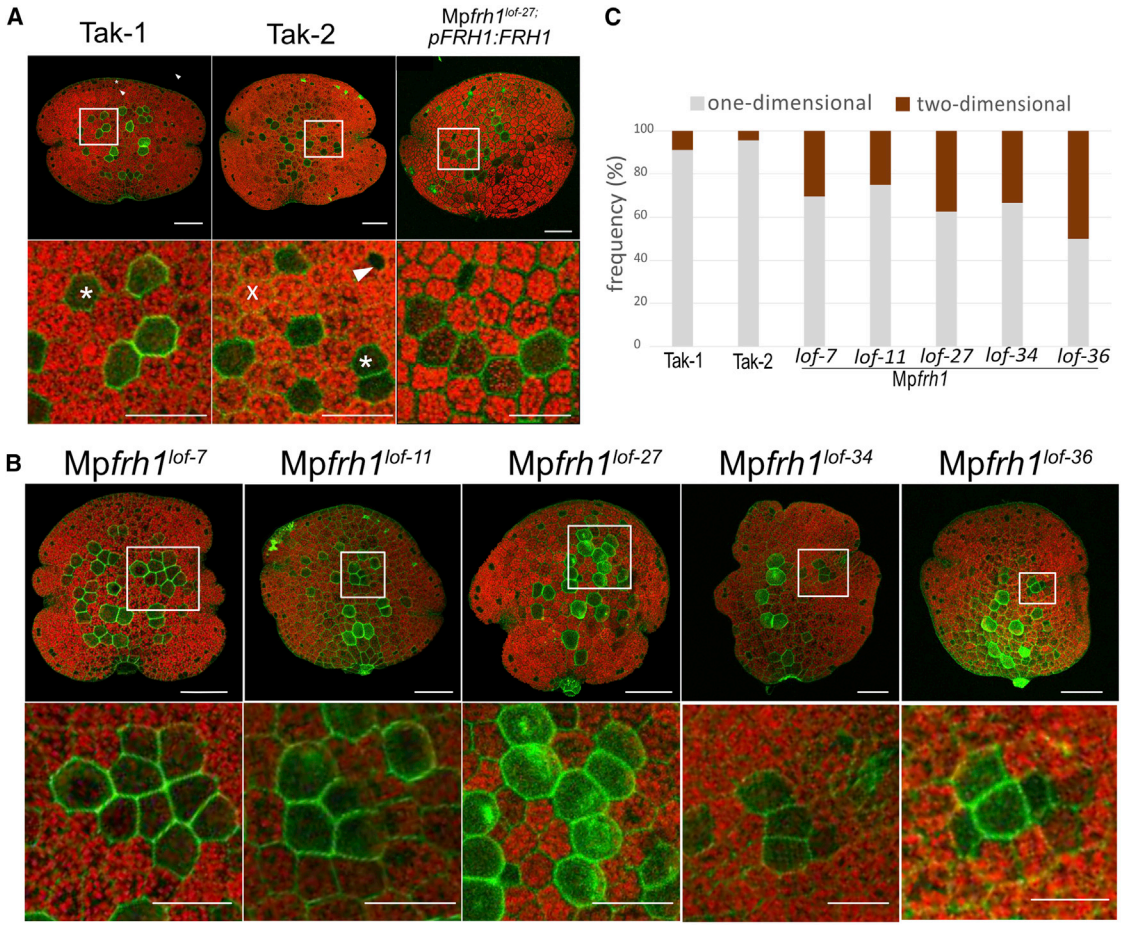

Figure 4. Two-Dimensional Rhizoid Cell Clusters Develop in Mp*frh1*^{lof} Mutants

(A) Rhizoid patterning in gemmae of wild type (Tak-1 and Tak-2) and Mp*frh1*$^{lof-27}$*;pFRH1:FRH1*. Upper row shows an overview of representative gemma (scale bar, 100 μm). Lower row shows a higher magnification of the inset highlighted above, showing representative rhizoid chains of wild type and a one-dimensional 5-cell chain of Mp*frh1*$^{lof-27}$*;pFRH1:FRH1* (scale bar, 50 μm). Asterisks indicate a rhizoid cell, x indicates a flat epidermal cell, and the arrowhead indicates an oil body cell.
(B) Rhizoid patterning in gemmae of Mp*frh1*$^{lof-7}$, Mp*frh1*$^{lof-11}$, Mp*frh1*$^{lof-27}$, Mp*frh1*$^{lof-34}$, and Mp*frh1*$^{lof-36}$ mutants. Upper row shows an overview of representative gemma (scale bar, 100 μm). Lower row shows a higher magnification of the highlighted square showing a representative rhizoid cluster (scale bar, 50 μm).
(C) Frequency (in %) of one-dimensional chains and two-dimensional clusters in wild type (Tak-1 and Tak-2) and Mp*frh1*^{lof} mutants, respectively. All rhizoid cell groups larger than 3 cells were combined (n[Tak-1] = 23, n[Tak-2 = 23], n[Mp*frh1*$^{lof-7}$] = 46, n[Mp*frh1*$^{lof-11}$] = 28, n[Mp*frh1*$^{lof-27}$] = 24, n[Mp*frh1*$^{lof-34}$] = 9, and n [Mp*frh1*$^{lof-36}$] = 8).

one-dimensional chains as in wild type. Remarkably, our simple model predicted similar shifts in both the mean and SD under loss of the purported lateral inhibition (Figure 2F).

To confirm that the increased number of rhizoid cell neighbors resulted in an increased frequency of two-dimensional clusters, as predicted by the model, we measured the frequency of one-dimensional and two-dimensional rhizoid groups in Mp*frh1*^{lof} mutants. In wild type, 92%–96% of rhizoid groups are one-dimensional chains, with only 4%–8% of rhizoid groups forming two-dimensional clusters. By contrast, 68% of rhizoid groups are one-dimensional chains and 32% of rhizoid groups are two-dimensional clusters in Mp*frh1*^{lof} mutants. This includes 30% of rhizoid clusters in Mp*frh1*$^{lof\ 7}$ (14 of 46), 25% in Mp*frh1*$^{lof-11}$ (7 of 21), 37% in Mp*frh1*$^{lof-27}$ (9 of 24), 33% in Mp*frh1*$^{lof-34}$ (3 of 9), and 50% in Mp*frh1*$^{lof-36}$ (4 of 8 cluster) (Figure 4C). The higher frequency of two-dimensional clusters in Mp*frh1*^{lof} than in wild type is consistent with the hypothesis that MpFRH1 activity is required for lateral inhibition during rhizoid development.

If MpFRH1 miRNA acts as an inhibitor during lateral inhibition, then the model predicted that rhizoid cell groups could be larger than 7, which is the largest rhizoid cell group observed in wild type. Up to 12 rhizoid cells could develop infrequently in Mp*frh1*^{lof} mutants. Such large groups could form from the merger of adjacent (smaller) rhizoid cell groups, a process that is inhibited in wild-type conditions. Rhizoid cell groups with more than 7 cells were found in Mp*frh1*^{lof} mutants (Table 1; Figure 4B). A single 8-rhizoid cell group and three 9-rhizoid cell groups were observed in Mp*frh1*$^{lof-7}$, and a single 8-rhizoid cell group was found in Mp*frh1*$^{lof-27}$. The observation that rare clusters containing up to 9 rhizoid cells developed in Mp*frh1*^{lof} mutants is consistent with the hypothesis that MpFRH1 acts as an inhibitor in lateral inhibition during epidermal development.

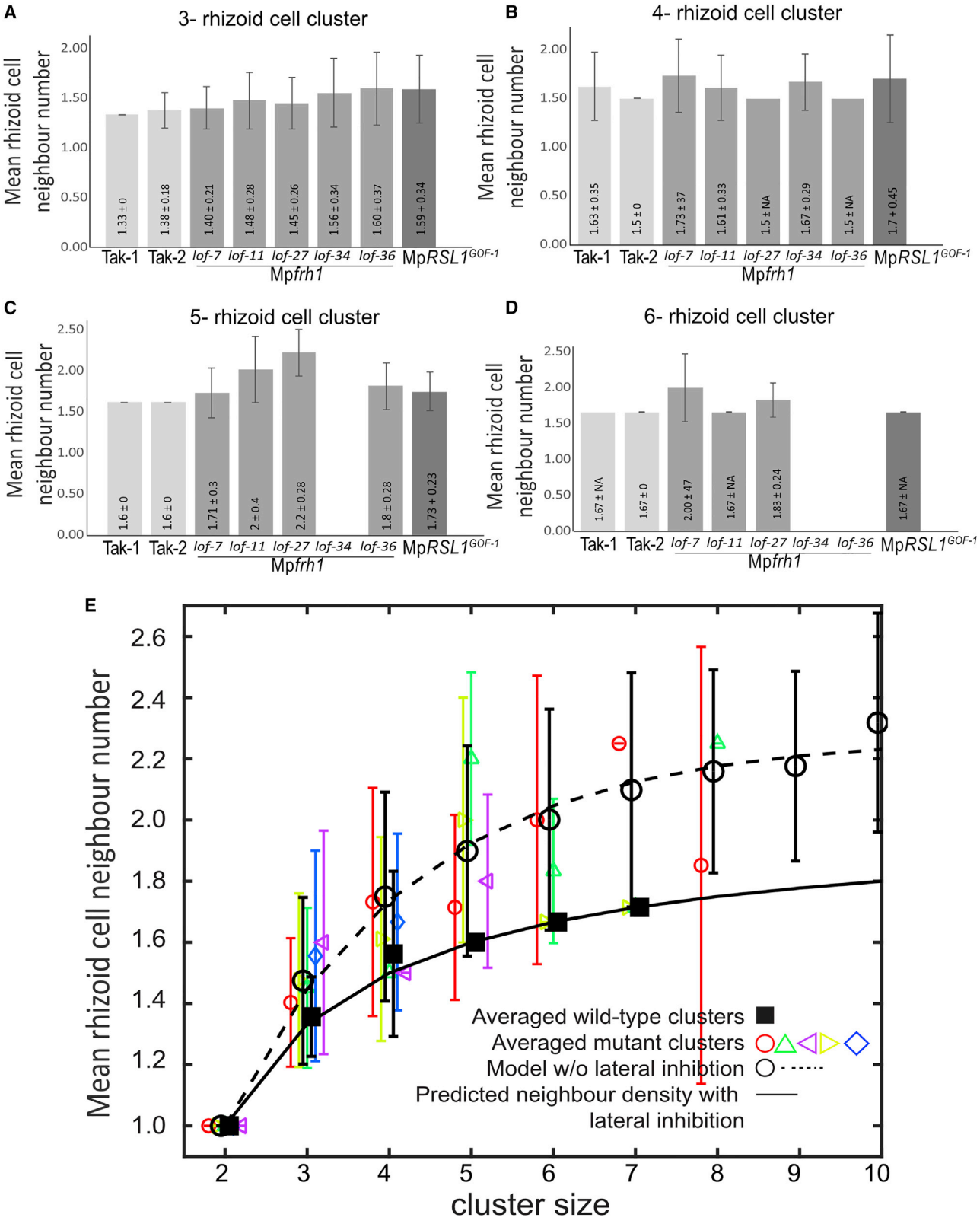

Figure 5. More Rhizoid Cell Neighbors Develop in Mp*frh1*^{lof} and Mp*RSL1*^{GOF} Mutants

(A–D) Mean rhizoid cell neighbor number in 3-rhizoid cell groups (A), 4-rhizoid cell groups (B), 5-rhizoid cell groups (C), and 6-rhizoid cell groups (D) in wild type (Tak-1 and Tak-2), Mp*frh1*$^{lof\text{-}7}$, Mp*frh1*$^{lof\text{-}11}$, Mp*frh1*$^{lof\text{-}27}$, Mp*frh1*$^{lof\text{-}34}$, Mp*frh1*$^{lof\text{-}36}$, and Mp*RSL1*$^{GOF\text{-}1}$. Error bars represent ± SD.

(legend continued on next page)

MpFRH1-Mediated Lateral Inhibition Acts by Repressing MpRSL1 Activity

Since MpFRH1 miRNA targets the Mp*RSL1* mRNA, we hypothesized that the loss of MpFRH1 function would result in an increase in steady-state levels of Mp*RSL1* mRNA. mRNA was isolated from thallus that developed from whole gemmae grown for 7 days. Mp*RSL1* mRNA abundance was normalized to the Mp*APT1* housekeeping gene [20]. Steady-state levels of Mp*RSL1* mRNA were higher in Mp*frh1*^{lof} mutants than in wild type. Steady-state levels of Mp*RSL1* mRNA were 2–2.5 times more abundant in Mp*frh1*$^{lof\text{-}36}$ and Mp*frh1*$^{lof\text{-}34}$ than in wild type (Figure 3C). Steady-state levels of Mp*RSL1* mRNA were ~1.5 times higher in Mp*frh1*$^{lof\text{-}7}$, Mp*frh1*$^{lof\text{-}11}$, and Mp*frh1*$^{lof\text{-}27}$ mutants than in wild type. In an independent experiment with fewer replicates, steady-state levels of Mp*RSL1* mRNA were 3.7-, 2.7-, 4.23-, 3.77-, and 1.6-fold higher in Mp*frh1*$^{lof\text{-}7}$, Mp*frh1*$^{lof\text{-}11}$, Mp*frh1*$^{lof\text{-}27}$, Mp*frh1*$^{lof\text{-}34}$, and Mp*frh1*$^{lof\text{-}36}$, respectively, than in wild type (Figure S3). These higher steady state levels in Mp*RSL1* mRNA in Mp*frh1*^{lof} mutants than in wild type is consistent with the hypothesis that MpFRH1 targets Mp*RSL1* mRNA during lateral inhibition.

If MpFRH1-mediated lateral inhibition operates by repressing MpRSL1, overexpression of MpRSL1 should overcome the inhibitory effect of MpFRH1. If true, ectopic overexpression of MpRSL1 would increase the mean number of rhizoid cell neighbors in rhizoid cell groups compared to wild type and larger groups of rhizoid cells would develop than in wild type. That is, the rhizoid cluster phenotypes of the Mp*RSL1*$^{GAIN\text{-}OF\text{-}FUNCTION\ (GOF)}$ and Mp*frh1*^{lof} mutants would be similar. A transfer DNA (T-DNA) insertion in the Mp*RSL1* promoter of the Mp*RSL1*$^{GOF\text{-}1}$ mutant causes overexpression of Mp*RSL1* [13]. 3-rhizoid cell clusters in Mp*RSL1*$^{GOF\text{-}1}$ mutants developed an average of 1.59 (SD = 0.34, n = 13) neighboring rhizoid cells compared to 1.36 neighbors in wild type (SD = 0.13) (Figure 5A). 4-rhizoid cell clusters in Mp*RSL1*$^{GOF\text{-}1}$ mutants developed 1.70 (SD = 0.45, n = 5) rhizoid cell neighbors compared to 1.58 in wild type (SD = 0.28) (Figure 5B). 5-rhizoid cell clusters in Mp*RSL1*$^{GOF\text{-}1}$ mutants developed 1.73 (SD = 0.23) neighbors compared to 1.60 in wild type (SD = 0) (Figure 5C). The larger number and variability of rhizoid cell neighbors in Mp*RSL1*$^{GOF\text{-}1}$ mutants than in wild type indicate that ectopic overexpression of Mp*RSL1* causes similar phenotypic defects in the spatial arrangement of rhizoid cells groups as in Mp*frh1*^{lof} mutants. These data are consistent with the hypothesis that MpFRH1 miRNA represses Mp*RSL1* activity during lateral inhibition as rhizoids develop. Rhizoids did not develop in either Mp*FRH1*$^{GOF\text{-}2}$ or Mp*rsl1*$^{lof\text{-}1}$, highlighting the essential function of MpRSL1 during rhizoid formation and the influence of MpFRH1 activity during rhizoid formation (Figure 6)

The model predicted that some two-dimensional rhizoid clusters induced by the absence of lateral inhibition would contain more than 7 cells (the maximum number of cells observed in a wild-type rhizoid group of cells). Furthermore, overexpression of Mp*RSL1* in Mp*RSL1*$^{GOF\text{-}1}$ mutants should overcome the effects of lateral inhibition. We therefore hypothesized that there would be more than 7 rhizoid cells in some clusters that develop in plants that ectopically overexpress Mp*RSL1*. There were up to 21 rhizoid cells in a single rhizoid cell cluster in Mp*RSL1*$^{GOF\text{-}1}$ plants (Figure S4). We observed three rhizoid cell clusters with more than 9 cells (a 10-cell cluster, a 12-cell cluster, and a 21-cell cluster; summarized as a $\geq$10-cell cluster in Table 1). This confirms that repression of Mp*RSL1* occurs during lateral inhibition. Taken together, the data reported here demonstrate that MpFRH1 is a repressor that acts during lateral inhibition and that MpFRH1 miRNA-mediated lateral inhibition acts by repressing Mp*RSL1* during the development of rhizoid cells in the *M. polymorpha* epidermis.

DISCUSSION

We discovered that MpFRH1 miRNA is a repressor that mediates lateral inhibition during *M. polymorpha* epidermis pattern formation. Rhizoid cells develop individually or as one-dimensional groups of cells of between 2 and 7 rhizoid cells in the wild-type epidermis in our growth conditions. There is a high frequency of single rhizoid cells and progressively fewer groups with 2, 3, 4, 5, 6, and 7 rhizoid cells. The spatial arrangement and distribution of rhizoid cells can be accounted for by a simple cellular automata model that includes lateral inhibition. This model allowed us to predict the phenotype of rhizoid cell patterns that would develop in a mutant in which lateral inhibition was absent. It predicted that rhizoid cells would develop in two-dimensional clusters in mutants with defective lateral inhibition compared to one-dimensional chains in wild type. It also predicted that the maximum cell number in rhizoid cell groups would be greater in the mutant than in wild type. We showed that the rhizoid cell phenotypes that develop in plants that lack the MpFRH1 miRNA are those predicted by the model for an epidermis developing without lateral inhibition; there were two-dimensional rhizoid cell clusters and rhizoid cell groups of up to 9 cells in the largest mutant rhizoid cell cluster compared to 7 in wild type. These combined modeling and genetic data indicate that lateral inhibition mediated by MpFRH1 miRNA is required for the patterning of rhizoid cells in *M. polymorpha*.

We propose that the development of rhizoid cells involves two distinct phases. The first phase involves the specification of individual rhizoid cells from a field of equivalent cells. The probability of a rhizoid cell being specified could be determined by stochastic variation in the expression levels of MpRSL1; higher levels would favor rhizoid cell development, and relatively lower levels would favor flat epidermal cell development. MpRSL1 then induces expression of the MpFRH1 miRNA in the developing rhizoid cell. MpFRH1 activity represses rhizoid cell development in adjacent cells through lateral inhibition, and these cells develop as flat epidermal cells. Repeated rounds of rhizoid initiation during a competence period results in the development of rare adjacent rhizoid cells that form groups of one-dimensional

(E) Comparison of theoretical predictions with experiments for rhizoid neighbor cell numbers of mutant and wild-type rhizoid cell groups. Shown is the experimentally observed relationship between mean rhizoid cell neighbor numbers and group size in wild type (filled black square) and Mp*frh1*^{lof} mutants (Mp*frh1*$^{lof\text{-}7}$ = red circle, Mp*frh1*$^{lof\text{-}11}$ = yellow triangle, Mp*frh1*$^{lof\text{-}27}$ = green triangle, Mp*frh1*$^{lof\text{-}34}$ = blue diamond, Mp*frh1*$^{lof\text{-}36}$ = purple triangle). Error bars represent SD. Black open circles on the dashed line represent the simulation results for the model without lateral inhibition (error bars represent SD from n = 1,000 simulations; the dashed line is the same line as shown in Figure 2F).

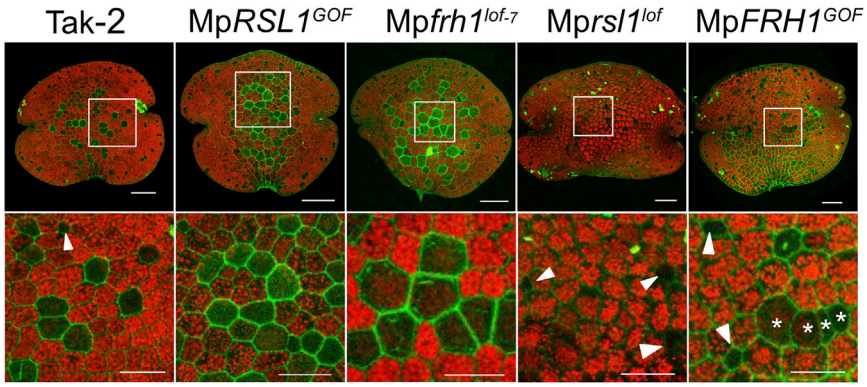

Figure 6. Larger Rhizoid Cell Clusters with Altered Shape Develop in Mp*frh1*^{lof} and Mp*RSL1*^{GOF} Mutants than in Wild Type

Upper row shows the distribution of rhizoid cells and rhizoid cell groups on representative mature gemmae of wild type (Tak-2) and Mp*RSL1*$^{GOF-1}$, Mp*frh1*$^{lof-7}$, Mp*rsl1*$^{lof-1}$, and Mp*FRH1*$^{GOF-2}$ mutants. Scale bar, 100 μm. The lower row shows a higher magnification of the inset highlighted on the image in the row above. There are 12 rhizoid cells in the Mp*RSL1*$^{GOF-1}$ rhizoid cell cluster and 8 cells in the Mp*frh1*$^{lof-7}$ rhizoid cell cluster. There are no rhizoids in the Mp*rsl1*$^{lof-1}$ mutants. Mp*FRH1*$^{GOF-2}$ mutants can rarely develop rhizoids, and one such rhizoid is indicated with asterisks. Chlororphyll autofluorescence is red, and cell walls of rhizoids are stained with propidium iodide (green). Scale bar, 50 μm. White arrowhead indicates the location of oil body cells. An exceptional 21-rhizoid cell cluster that developed in Mp*RSL1*$^{GOF-1}$ is shown in Figure S6.

chains, and the shape of these rhizoid cell groups is determined by lateral inhibition.

Our modeling and experimental data suggest that being adjacent to 2 rhizoid cells represses rhizoid cell development. By contrast, being adjacent to a single rhizoid cell is not sufficient to repress rhizoid development. This suggests that there is a threshold of repressor activity. Being adjacent to 1 rhizoid cell exposes an adjacent cell to sub-threshold levels of repressor, while being adjacent to 2 rhizoid cells exposes a cell to repressor levels above this threshold and represses differentiation. A repressive signal from a rhizoid cell to adjacent cells represses rhizoid cell development if it reaches a threshold level in the receiving cell. We show that MpFRH1 activity is required for this repressive signal. There are at least three potential modes of signaling that could operate in this system. First, the repressive signal could be MpFRH1 miRNA itself. miRNAs can be mobile, and it has been suggested that movement of miRNAs can account for the establishment of tissue boundaries in organs [21]. Second, the repressive signal could be produced as a result of MpFRH1 miRNA activity. Since MpRSL1 mRNA is the only confirmed target of MpFRH1, the production of this hypothetical signal would likely also be MpRSL1 dependent [14]. Third, the repressive signal could be transmitted by cell contact through an unknown mechanism. The amount of contact could be proportional to the total cell-surface area shared between neighboring cells. Accordingly, sharing a single cell face would expose the cells to sub-threshold levels of repressor, while sharing a cell face with 2 rhizoid cells would expose the cell to repressor levels above this threshold. Since Mp*RSL1* mRNA is the only confirmed target of MpFRH1, the production of this hypothetical cell-contact signal would also be MpRSL1 dependent.

While the molecular mechanisms of lateral inhibition are different between plants (transcriptional regulator, EDP2, and MpFRH1 dependent) and metazoans (Delta-Notch), there are similarities in the underlying logic of the process. For example, the Delta ligand represses neuroblast development during Notch-Delta signaling in *Drosophila* (reviewed in [2]). However, Delta is expressed on future neuroblasts and represses neuroblast development in adjacent cells by non-cell-autonomous signaling mediated by the Notch receptor located on the neighboring cell. That is, the repressor acts at a distance from its site of synthesis to repress the neuroblast cell identity in adjacent cells. This logic operates in Myb-repressor- and EDP2-mediated lateral inhibition of trichomes and guard cells, respectively, in *A. thaliana*. Similar logic operates in MpFRH1-mediated lateral inhibition in *M. polymorpha*. MpFRH1 is a repressor of rhizoid cell development that it is expressed in developing rhizoid cells. Furthermore, our data indicate that MpFRH1 miRNA represses rhizoid cell identity in adjacent cells that would otherwise differentiate as flat epidermal cells in wild type. This leads to the hypothesis that MpFRH1 expression in developing rhizoid cells acts non-cell autonomously to repress rhizoid cell development in epidermal cells next to rhizoid cells. While the molecular mechanism of lateral inhibition is different between plants and animals, the regulatory similarities suggest that there may be underlying similarities in control logic.

Mechanisms that pattern different cell types in the epidermis and do not involve lateral inhibition also exist in plants. These include the development of pattern in the root epidermis and giant cells in sepals of *A. thaliana*. Mobile transcription factors are involved in the patterning of cells that are not initially equivalent in the root epidermis (reviewed in [22]). The cells that form root hair cells (trichoblasts) perceive different positional information than those that develop as non-hair-bearing epidermal cells (atrichoblasts) in *A. thaliana* [23]. Therefore, the intercellular signaling mechanism that patterns the distribution of root hair cells and non-root hair cells builds on an existing pattern that already exists. There is evidence that signaling that leads to positionally defined development of these two cell types is mediated by the SCRAMBLED receptor protein and requires the activity of the JACKDAW transcription factor in subepidermal cells [24–28]. Cell-to-cell signaling is involved in giant cell development of the sepal epidermis, but there is no evidence for lateral inhibition. The sepal epidermis comprises a few giant cells distributed among pavement epidermal cells; ~14 giant cells develop on each sepal, and these can run 20% the length of the entire organ. The pattern of giant cells among pavement epidermal cells is determined by relative rates of cell division in the two cell types during development [29, 30]. As the sepal grows, giant cells stop dividing but continue to grow while surrounding cells divide. Activation of an cyclin-dependent kinase (CDK) called LOSS OF GIANT CELLS FROM ORGANS (LGO) in developing giant cells promotes endoreduplication and blocks mitosis [29, 31]. The specification of giant cells requires the expression of the

MERISTEM LAYER 1 (ML1) transcription factor, while neighboring epidermal cells do not express ML1 [29, 32]. To date, there is no evidence that the distribution of ML1-expressing future giant cells requires lateral inhibition. However, giant cell specification requires the DEFECTIVE KERNAL1 (DEK1) calpain protease and the *ARABIDOPSIS* CRINKLY KINASE (ACR4) receptor, suggesting that cell-to-cell signaling may act early in the process [29]. It is therefore formally possible that DEK and ACR4 proteins could mediate lateral inhibition during the patterning of giant cells. If so, these proteins would likely act transiently, early in development.

The MpRSL1-MpFRH1 mechanism of lateral inhibition that controls the patterning of rhizoid cells is liverwort specific. MpFRH1 is a liverwort-specific miRNA, and the miRNA target sequence has been identified in the RSL genes of many liverwort taxa but has not been found in RSL genes from any other lineage of land plants [14]. This indicates that the mechanism of lateral inhibition in the liverwort lineage is entirely different from the two mechanisms that have been described among the angiosperms (Myb repressor and EPF2). The MpFRH1-lateral inhibition mechanism is restricted to the liverworts, suggesting that different lateral inhibition mechanisms control the patterning of tip-growing rooting cells, rhizoids, and root hairs in liverworts and angiosperms, respectively. It also demonstrates that entirely different mechanisms can operate to control lateral inhibition in early-diverging groups of land plants (hornworts and mosses) than in angiosperms. This contrasts with animals in which the Notch-Delta mechanism of lateral inhibition is conserved among metazoan lineages. We propose that different mechanisms of lateral inhibition evolved many times during the course of land plant evolution, while a single mechanism has been conserved among metazoans.

STAR★METHODS

Detailed methods are provided in the online version of this paper and include the following:

- KEY RESOURCES TABLE
- LEAD CONTACT AND MATERIALS AVAILABILITY
- EXPERIMENTAL MODEL AND SUBJECT DETAILS
- METHOD DETAILS
  - CRISPR/Cas9 knock out
  - Generation of Mpfrh1$^{lof\text{-}27}$pFRH1:FRH1 transgenic line
  - qPCR of MpRSL1 and MpAPT
  - Stem loop PCR for MpFRH1 and MpmiR166
  - Imaging
  - Modeling
- QUANTIFICATION AND STATISTICAL ANALYSIS
- DATA AND CODE AVAILABILITY

SUPPLEMENTAL INFORMATION

Supplemental Information can be found online at https://doi.org/10.1016/j.cub.2020.03.032.

ACKNOWLEDGMENTS

Vector pHB453 was generated by Holger Breuninger after discussion with Julius Durr, Jose Gutierrez-Marcos, and H. Puchta. T.E.S. and L.D. are grateful to the Kavli Institute, Santa Barbara, which supported their visits to the institute, supported in part by NSF grant PHY-1748958, NIH grant R25GM067110, and Gordon and Betty Moore Foundation grant 2919.01. T.E.S. acknowledges support from the Mechanobiology Institute and a Human Frontiers Young Investigator grant (RGY0083/2016). L.D. is funded by a European Research Council advanced grant (Denovo-P, contract 787613). A.T. was funded by the Biotechnology and Biological Sciences Research Council (BBSRC) (BB/J014427/1) and an Edward Penley Abraham Cephalosporin Scholarship.

AUTHOR CONTRIBUTIONS

L.D. and A.T. formulated the project. A.T. generated and characterized the Mp*frh1*^{lof} mutants and acquired all quantitative data. T.E.S. performed the mathematical modeling. L.D. wrote the paper, with input from all authors.

DECLARATION OF INTERESTS

The authors declare no competing interests.

Received: December 3, 2019
Revised: February 18, 2020
Accepted: March 12, 2020
Published: April 2, 2020

REFERENCES

1. Artavanis-Tsakonas, S., Matthew, D.,R., and Robert, J.,L. (1999). Notch signaling: cell fate control and signal integration in development. Science *284*, 770–776.
2. Bray, S.J. (2006). Notch signalling: a simple pathway becomes complex. Nat. Rev. Mol. Cell Biol. *7*, 678–689.
3. Perrimon, N., Pitsouli, C., and Shilo, B.Z. (2012). Signaling mechanisms controlling cell fate and embryonic patterning. Cold Spring Harb. Perspect. Biol. *4*, a005975.
4. Arabidopsis Genome Initiative (2000). Analysis of the genome sequence of the flowering plant Arabidopsis thaliana. Nature *408*, 796–815.
5. Wigge, P.A., and Weigel, D. (2001). *Arabidopsis* genome: life without notch. Curr. Biol. *11*, R112–R114.
6. Bowman, J.L., Kohchi, T., Yamato, K.T., Jenkins, J., Shu, S., Ishizaki, K., Yamaoka, S., Nishihama, R., Nakamura, Y., Berger, F., et al. (2017). Insights into land plant evolution garnered from the *Marchantia polymorpha* genome. Cell *171*, 287–304.e15.
7. Horst, R.J., Fujita, H., Lee, J.S., Rychel, A.L., Garrick, J.M., Kawaguchi, M., Peterson, K.M., and Torii, K.U. (2015). Molecular framework of a regulatory circuit initiating two-dimensional spatial patterning of stomatal lineage. PLoS Genet. *11*, e1005374.
8. Lee, J.S., Hnilova, M., Maes, M., Lin, Y.C.L., Putarjunan, A., Han, S.K., Avila, J., and Torii, K.U. (2015). Competitive binding of antagonistic peptides fine-tunes stomatal patterning. Nature *522*, 439–443.
9. Simmons, A.R., and Bergmann, D.C. (2016). Transcriptional control of cell fate in the stomatal lineage. Curr. Opin. Plant Biol. *29*, 1–8.
10. Schellmann, S., Schnittger, A., Kirik, V., Wada, T., Okada, K., Beermann, A., Thumfahrt, J., Jürgens, G., and Hülskamp, M. (2002). TRIPTYCHON and CAPRICE mediate lateral inhibition during trichome and root hair patterning in *Arabidopsis*. EMBO J. *21*, 5036–5046.
11. Menand, B., Yi, K., Jouannic, S., Hoffmann, L., Ryan, E., Linstead, P., Schaefer, D.G., and Dolan, L. (2007). An ancient mechanism controls the development of cells with a rooting function in land plants. Science *316*, 1477–1480.
12. Catarino, B., Hetherington, A.J., Emms, D.M., Kelly, S., and Dolan, L. (2016). The stepwise increase in the number of transcription factor families in the precambrian predated the diversification of plants on land. Mol. Biol. Evol. *33*, 2815–2819.
13. Proust, H., Honkanen, S., Jones, V.A.S., Morieri, G., Prescott, H., Kelly, S., Ishizaki, K., Kohchi, T., and Dolan, L. (2016). RSL class I genes controlled

the development of epidermal structures in the common ancestor of land plants. Curr. Biol. *26*, 93–99.

14. Honkanen, S., Thamm, A., Arteaga-Vazquez, M.A., and Dolan, L. (2018). Negative regulation of conserved *RSL* class I bHLH transcription factors evolved independently among land plants. eLife *7*, e38529.
15. Hwang, M., Garbey, M., Berceli, S.A., and Tran-Son-Tay, R. (2009). Rule-based simulation of multi-cellular biological systems: a review of modeling techniques. Cell. Mol. Bioeng. *2*, 285–294.
16. Glen, C.M., Kemp, M.L., and Voit, E.O. (2019). Agent-based modeling of morphogenetic systems: advantages and challenges. PLOS Comput. Biol. *15*, e1006577.
17. Piotrowska, M.J., and Angus, S.D. (2009). A quantitative cellular automaton model of in vitro multicellular spheroid tumour growth. J. Theor. Biol. *258*, 165–178.
18. Palsson, E. (2008). A 3-D model used to explore how cell adhesion and stiffness affect cell sorting and movement in multicellular systems. J. Theor. Biol. *254*, 1–13.
19. Sugano, S.S., Shirakawa, M., Takagi, J., Matsuda, Y., Shimada, T., Hara-Nishimura, I., and Kohchi, T. (2014). CRISPR/Cas9-mediated targeted mutagenesis in the liverwort *Marchantia polymorpha* L. Plant Cell Physiol. *55*, 475–481.
20. Saint-Marcoux, D., Proust, H., Dolan, L., and Langdale, J.A. (2015). Identification of reference genes for real-time quantitative PCR experiments in the liverwort *Marchantia polymorpha*. PLoS ONE *10*, e0118678.
21. Carlsbecker, A., Lee, J.-Y., Roberts, C.J., Dettmer, J., Lehesranta, S., Zhou, J., Lindgren, O., Moreno-Risueno, M.A., Vatén, A., Thitamadee, S., et al. (2010). Cell signalling by microRNA165/6 directs gene dose-dependent root cell fate. Nature *465*, 316–321.
22. Dolan, L. (2006). Positional information and mobile transcriptional regulators determine cell pattern in the *Arabidopsis* root epidermis. J. Exp. Bot. *57*, 51–54.
23. Berger, F., Hung, C.Y., Dolan, L., and Schiefelbein, J. (1998). Control of cell division in the root epidermis of *Arabidopsis thaliana*. Dev. Biol. *194*, 235–245.
24. Lee, M.M., and Schiefelbein, J. (2002). Cell pattern in the *Arabidopsis* root epidermis determined by lateral inhibition with feedback. Plant Cell *14*, 611–618.
25. Savage, N.S., Walker, T., Wieckowski, Y., Schiefelbein, J., Dolan, L., and Monk, N.A.M. (2008). A mutual support mechanism through intercellular movement of CAPRICE and GLABRA3 can pattern the *Arabidopsis* root epidermis. PLoS Biol. *6*, e235.
26. Kwak, S.-H., Shen, R., and Schiefelbein, J.W. (2005). Positional signaling mediated by a receptor-like kinase in Arabidopsis. Science *307*, 1111–1113.
27. Kwak, S.H., and Schiefelbein, J. (2007). The role of the SCRAMBLED receptor-like kinase in patterning the *Arabidopsis* root epidermis. Dev. Biol. *302*, 118–131.
28. Hassan, H., Scheres, B., and Blilou, I. (2010). JACKDAW controls epidermal patterning in the *Arabidopsis* root meristem through a non-cell-autonomous mechanism. Development *137*, 1523–1529.
29. Roeder, A.H.K., Cunha, A., Ohno, C.K., and Meyerowitz, E.M. (2012). Cell cycle regulates cell type in the *Arabidopsis* sepal. Development *139*, 4416–4427.
30. Robinson, D.O., and Roeder, A.H.K. (2015). Themes and variations in cell type patterning in the plant epidermis. Curr. Opin. Genet. Dev. *32*, 55–65.
31. Roeder, A.H.K., Chickarmane, V., Cunha, A., Obara, B., Manjunath, B.S., and Meyerowitz, E.M. (2010). Variability in the control of cell division underlies sepal epidermal patterning in *Arabidopsis thaliana*. PLoS Biol. *8*, e1000367.
32. Meyer, H.M., Teles, J., Formosa-Jordan, P., Refahi, Y., San-Bento, R., Ingram, G., Jönsson, H., Locke, J.C.W., and Roeder, A.H.K. (2017). Fluctuations of the transcription factor ATML1 generate the pattern of giant cells in the *Arabidopsis* sepal. eLife *6*, 1–41.
33. Ishizaki, K., Chiyoda, S., Yamato, K.T., and Kohchi, T. (2008). *Agrobacterium*-mediated transformation of the haploid liverwort *Marchantia polymorpha* L., an emerging model for plant biology. Plant Cell Physiol. *49*, 1084–1091.
34. Ruijter, J.M., Ramakers, C., Hoogaars, W.M.H., Karlen, Y., Bakker, O., van den Hoff, M.J., and Moorman, A.F. (2009). Amplification efficiency: linking baseline and bias in the analysis of quantitative PCR data. Nucleic Acids Res. *37*, e45.
35. Schindelin, J., Arganda-Carreras, I., Frise, E., Kaynig, V., Longair, M., Pietzsch, T., Preibisch, S., Rueden, C., Saalfeld, S., Schmid, B., et al. (2012). Fiji: an open-source platform for biological-image analysis. Nat. Methods *9*, 676–682.
36. Honkanen, S., Jones, V.A.S., Morieri, G., Champion, C., Hetherington, A.J., Kelly, S., Proust, H., Saint-Marcoux, D., Prescott, H., and Dolan, L. (2016). The mechanism forming the cell surface of tip-growing rooting cells is conserved among land plants. Curr. Biol. *26*, 3238–3244.
37. Kubota, A., Ishizaki, K., Hosaka, M., and Kohchi, T. (2013). Efficient Agrobacterium-mediated transformation of the liverwort *Marchantia polymorpha* using regenerating thalli. Biosci. Biotechnol. Biochem. *77*, 167–172.
38. Varkonyi-Gasic, E., Wu, R., Wood, M., Walton, E.F., and Hellens, R.P. (2007). Protocol: a highly sensitive RT-PCR method for detection and quantification of microRNAs. Plant Methods *3*, 12.

STAR★METHODS

KEY RESOURCES TABLE

REAGENT or RESOURCE	SOURCE	IDENTIFIER
Bacterial and Virus Strains		
Escherichia coli One Shot OmniMAX 2 T1^{R}	Thermo Fisher Scientific	Cat.# C854003
Agrobacterium tumefaciens GV3101	Widely distributed	N/A
Chemicals, Peptides, and Recombinant Proteins		
Propidium Iodide	Thermo Fisher Scientific	Cat.# P1304MP
Johnson's growth medium	[33]	N/A
Hygromycin	Melford	CAS# 31282-04-9
BbsI	NEB	Cat.# R0539S
BsmBI	NEB	Cat.# R0580S
Gateway LR Clonase II Enzyme mix	Thermo Fisher Scientific	Cat.# 11791100
Cefotaxime	Melford	CAS# 64485-93-4
In-Fusion HD Cloning Kit	Takara	Cat # 639635
ProtoSript II Reverse Transcriptase	NEB	#M0368
Murine RNase Inhibitor	NEB	#M0314
PCRBIO Ultra Polymerase	PCR Biosystems	PB10.31-02
SYBR Safe DNA Gel Stain	Thermo Fisher Scientific	Cat.# S33102
Critical Commercial Assays		
Direct-Zol RNA MINIprep kit	Zymo Research	Cat.# R2050
TURBO DNA-free kit	Thermo Fisher Scientific	Product Code 10136824
SensiMix SYBR Hi-ROX Kit	bioline	Cat.# QT605-05
miRVana miRNA Isolation Kit	Thermo Fisher Scientific	Cat.# AM1560
Experimental Models: Organisms/Strains		
Marchantia polymorpha (Tak-1 and Tak-2)	Widely distributed	N/A
Genetically modified *M. polymorpha* - Mp*frh1*$^{lof\text{-}7/11/27/34/36}$	this paper	N/A
Genetically modified *M. polymorpha* - Mp*FRH1*$^{GOF\text{-}2}$ (ST49-10)	[14]	N/A
Genetically modified *M. polymorpha* - Mp*RSL1*$^{GOF\text{-}1}$	[13]	N/A
Genetically modified *M. polymorpha* – Mp*rsl1*$^{lof\text{-}1}$	[13]	N/A
Genetically modified *M. polymorpha* Mp*frh1*$^{lof\text{-}27}$*;pFRH1:FRH1*	this paper	N/A
Oligonucleotides		
oAT110 - CTCGCTAGCAGTTGCTGG AGTTCG	this paper	N/A
oAT111 - AAACCGAACTCCAGCAACTGCTAG	this paper	N/A
oAT112 - CTCGGATCCTCACCTTCCTCACAG	this paper	N/A
oAT113 - AAACCTGTGAGGAAGGTGAGGATC	this paper	N/A
oAT135 - GTACTTCCATCAGCAGACGACATCA	this paper	N/A
oAT136 - ATCTGCATCCTTCAGTGTCCCCT	this paper	N/A
oAT173/ MpRSL1-F - AGATGAGTCTGGGGCAACC	[13]	N/A
oAT174/ MpRSL1-R - GGATGAGCGCTTTAGAGTG	[13]	N/A
oAT175 - CGAAAGCCCAAGAAGCTACC	[20]	N/A
oAT176 - GTACCCCCGGTTGCAATAAG	[20]	N/A
oAT187- CAATTCCCGATCTAGTAACATAG	this paper	N/A
oAT194 - ATACGAACGAAAGCTGGCAAAGCAAATTTAT	this paper	N/A
oAT195 – GGCGCTCTTTCTCCCTCATCATTCGGCACTC	this paper	N/A
oAT196 – AGGGAGAAAGAGCGCCTGCG	this paper	N/A
oAT197 – AGCTTTCGTTCGTATCATC	this paper	N/A

(*Continued on next page*)

Continued

REAGENT or RESOURCE	SOURCE	IDENTIFIER
oAT198 – CGCTTCGACAGACGGAAAAC	this paper	N/A
oAT199 – GTTTTCCGTCTGTCGAAGCG	this paper	N/A
oAT218 – GTCGTATCCAGTGCAGGGTCCGAGG TATTCGCACTGGATACGACACATTG	[14]	N/A
oAT219 – GTCGTATCCAGTGCAGGGTCCGAGG TATTCGCACTGGATACGACGGGAAT	this paper – designed by S.Streubel	N/A
oAT220 - CCAGTGCAGGGTCCGAGGTA	[14]	N/A
oAT221 - CGGCGTGTGTGAGAAGAGGC	[14]	N/A
oAT222 - CGCTCTTCGGACCAGGCTTC	this paper – designed by S.Streubel	N/A
Software and Algorithms		
LinRegPCR v2012.0	[34]	http://LinRegPCR.HFRC.nl
MATLAB R2017b	MathWorks	https://www.mathworks.com/
Fiji	[35]	https://fiji.sc/
Affinity Designer	Serif Europe	https://affinity.serif.com/en-gb/designer/
Other		
cellulosic cellophane membrane	AA Packaging Limited, Preston, UK	N/A

LEAD CONTACT AND MATERIALS AVAILABILITY

Further information and requests for genetic stocks, gene constructs, resources and reagents reported in this publication should be directed to and will be provided by the Lead Contact, Liam Dolan (liam.dolan@plants.ox.ac.uk).

EXPERIMENTAL MODEL AND SUBJECT DETAILS

Marchantia polymorpha accessions Tagaragaike-1 (Tak-1, male) and Tagaragaike-2 (Tak-2, female) [33] were used as wild-type and grown on plates that were placed horizontally in a Sanyo growth cabinet at 23°C under continuous white light (56 μE.m-2 .s-1) as reported in [36]. Mp*RSL1*$^{GOF-1}$ and Mp*rsl1*$^{lof-1}$ (ST46-1) were generated by [13]. Mp*FRH1*$^{GOF-2}$ (ST49-10) was generated by [14]. Mp*frh1*^{lof} lines were generated in this study as reported below. For crossing, plants were grown in a growth chamber at 23°C under 16 hours light: 8 hours dark photoperiod on 1:3 mixture of vermiculite and John Innes No. 2 compost. Sexual reproduction was induced by far-red light irradiation. Spores for transformation were obtained from a cross between the wild-type lines Tak-1 and Tak-2 as reported in [36]. For RNA extraction plants were grown on medium covered with cellulosic cellophane membrane (AA Packaging Limited, Preston, UK) before harvesting to avoid agar contamination.

METHOD DETAILS

CRISPR/Cas9 knock out

CRISPR/Cas9 mutations were generated following the protocol described in [19]. A new sgRNA construct, called pHB453, using 2 sgRNA for the generation of deletions was generated and kindly provided by Holger Breuninger (University of Tübingen). The sgRNA design was based on pMpGE_En03 with a second pU6 driven sgRNA scaffold between the att sites. The first sgRNA scaffold harbors a BbsI restriction site and the second a BsmBI restriction site. Primer oAT110 and oAT111 were used to introduce sgRNA1 into the BbsI site, primer oAT112 and oAT113 were used to introduce sgRNA2 into BsmBI site to generate the entry vector pAT48. The expression vector, called pAT54, was generated by LR reaction of the destination vector pMpGE010 and the entry vector pAT48.

Vectors were transformed into *Escherichia coli* One Shot OmniMAX 2 T1^{R} strains. pAT54 was transformed into *Agrobacterium tumefaciens* GV3101. Transformation of haploid *M.polymorpha* spores was carried out as reported in [36]. Transformed sporelings were grown on antibiotic selection plates containing Johnson's medium with 10 mg/l hygromycin to select for plants with a T-DNA insertion, and 100 mg/l cefotaxime to kill the remaining Agrobacterium. To test for deletions at the MpFRH1 locus, the MpFRH1 allele was amplified using primer oAT135 and pAT136 and subsequentially sequenced by Source BioScience.

Generation of Mpfrh1^{lof-27}pFRH1:FRH1 transgenic line

Mp*frh1*$^{lof-27}$ was crossed to wild-type to generate a segregating population. First, plants in this segregating population that lacked the CRISPR.Cas9 transgene were identified. Lines lacking the T-DNA insertion harboring the CRISPR/Cas9 construct were selected by

screening for hygromycin sensitivity. Plants were cut in 2 and replica plated onto either Hygromicin-containing media or media with no Hygromycin added. Hygroomycin sensitive plants (grown without hygromycin) were genotyped by PCR using oAT110 and oAT187 primers which amplify the the CRISPR/Cas9 construct. Second, plants with the Mp*frh1*$^{lof\text{-}27}$ deletion were identified from the hygromycin-sensitive lines that lacked the CRISPR/Cas9 transgenes by genotyping using PCR with oAT135 abd oAT136 primers located in the Mp*FRH1* gene. To construct the transformation vector pAT82 (pFRH1:FRH1 in pCambia) the 1200 bp long MpFRH1 transcript was amplified from the MpFRH1 pri-miRNA overexpression constructs generated in [14] using oAT194 and oAT195. The backbone of pAT82 harboring the pFRH1 promoter and a Hygromycin resitance cassette from pCAMBIA was amplified from proMpFRH1:NLS-3xYFP generated in [14] in 2 pieces; the first amplicon was generated by PCR using oAT197 and pAT199 primers and the second amplicon generated by PCR using oAT196 and oAT198 primers. All 3 amplicons were spliced together using the In-Fusion HD Cloning Kit, following manufacturer's instructions. pAT82 was transformed into *Agrobacterium tumefaciens* GV3101, and this strain was used to transform Mp*frh1*$^{lof\text{-}27}$ mutant plants by thallus transformation as described in [37]. Positive transformants were selected for Hygromycin resistance and genotyped by PCR using oAT135/oAT136 primers.

qPCR of MpRSL1 and MpAPT

Total RNA was extracted from 7-day old gemmae using Direct-Zol RNA MINIprep kit (Zymo Research) following manufactures instructions. For each line 3 biological replicates were extracted unless stated otherwise. To remove DNA, 3ug total RNA were treated with TURBO DNA-free kit following manufacturers instruction. cDNA synthesis was performed according to the First Strand cDNA Synthesis protocol from NEB using ProtoSript II Reverse Transcriptase (#M0368) and Murine RNase Inhibitor (#M0314). MpRSL1 and MpAPT cDNA was amplified using the primer oAT173/oAT174 and oAT175/176, respectively (as previously reported in [14, 20]). qRT-PCT was performed in the Applied Biosystems 7300 Real-Time PCR System (Life Technologies) with SensiMix SYBR Hi-ROX Kit (Bioline, QT605-05) following manufactures instructions. 3 technical replicates per biological replicate were performed. qPCR data was first analyzed using LinRegPCR v2012.0 [34]. The average N0 value was calculated. Relative RSL1 mRNA abundance was calculated by normalizing the N0 of each replicate against the N0 value of the reference gene, MpAPT1.

Stem loop PCR for MpFRH1 and MpmiR166

To amplify MpFRH1 and MpmiR166, RNA was extracted from 19 day old gemmae using miRVana miRNA Isolation Kit following manufacturer's instructions. 1ug RNA was treated with DNase according to TURBO DNA-free kit following manufacturers instruction. Stem-loop PCR was carried out as described in [38] using a MpFRH1 specific primer (oAT218) or a MpmiR166 specific primer (oAT219). The reverse transcribed and extended miRNAs were amplified using PCRBIO Ultra Polymerase (PCR Biosystem, PB10.31-02) with a miRNA specific forward primer (oAT221 for MpFRH1, oAT222 for MpmiR166) and a universal reverse primer (oAT220). Amplicons were visualized on a 3% agarose gel containing SYBR Safe.

Imaging

Cell walls were stained using propidium iodide (PI). Gemmae were incubated in 5ug/ml PI solution for (5-)10 minutes. PI solution was removed and gemmae washed twice with MilliQ water. Gemmae were mounted on a slide with heated 0.2% agar solution. Once Agar solidified gemmae were imaged immediately. Images were acquired with a Leica SP5 confocal laser microscope and the Leica Application Suite (LAS) software using either a Leica HCX PL Fluotar 10x/0.30 or HC PL APO 20x/0.75 IMM CORR CS2 lense. PI and chlorophyll were excited at 543 nm and emission was collected between 561 and 640 nm for PI and between 680-700nm for chlorophyll.

Modeling

The cell automata model was implemented as follows. First, a grid of ~400 hexagonal cells was defined. A predefined density of cells were selected as rhizoid precursors (typically 10%–15%). Simulations were performed with hard-wall boundary conditions, similar to the restrictions in the leaf.

For each iteration of the simulation, a probability P defined the probability for whether a group of rhizoid cells added a new cell to the group. In this case, we define the group to be *active*. With probability (1-P) the group becomes *inactive*. Once inactive, the group remains inactive for the rest of the simulation. In each iteration of the simulation, each active rhizoid group was tested by drawing a uniform random number r between 0 and 1 ($r < P$, the rhizoid group adds a new cell from the neighboring non-rhizoid cell population; if $r > P$, then the group becomes inactive). The simulation repeated this process until all rhizoid cell groups finished expansion – i.e., all groups are inactive. In this simple scenario, the probability of a group having n cells = $(1\text{-}P)^n$.

When a group of cells is selected for expansion, two possible rules were considered. (1) No lateral inhibition; in this case, any neighboring cell to the rhizoid cell group can become integrated with the group. (2) With lateral inhibition; only cells neighboring exactly 1 member of the rhizoid group can become integrated within the group. We also considered the restriction that the new rhizoid cell has to be a neighbor of an end cell of the group. This corresponds to 4 possible configurations: (i) lateral inhibition with only end joining; (ii) lateral inhibition with new cells allowed so long as only 1 neighbor in the rhizoid group (see hatched cell in Figure 2A); (iii) no lateral inhibition with only end joining; (iv) no lateral inhibition with new cells allowed so long as only 1 neighbor in the rhizoid group. The results presented in the paper for wild-type and mutants correspond to cases (i) and (iv) respectively. However, using rules (ii) and (iii) do not alter the general results, though the wild-type rhizoid group can become more irregular as branching can occur. In each simulation, once a group is found to expand, then the available possible cells for expansion are identified – this choice is

restricted by the 4 possible configurations outlined above. The *n* available cells are labeled *1,2,…,n*. A random integer between [1, n] is then generated by the computer to select the cell that becomes a member of the rhizoid group. Examples of the simulation iterations are shown in Figure S2.

When lateral inhibition was present, 2 nearby rhizoid cell groups cannot merge; any cell between 2 groups would have a minimum of 2 rhizoid neighbors and groups of rhizoid cells are arranged in one-dimensional chains. In the absence of lateral inhibition, such a cell can take on the rhizoid cell fate. Hence, 2 groups can merge to form a larger 2-dimensional cluster. In this way, although *P* is unchanged in all simulations, large 2-dimensional clusters are possible in the absence of lateral inhibition.The model was encoded in MATLAB R2017b. All data is produced from averaging the average cluster distributions for 1000 simulations, each with different initial distribution of rhizoids.

In Figure 2F, the fit $1+1.27[1-\exp(-((N-2)/2.3))]$ to the case without lateral inhibition was performed using the MATLAB function *fit*.

QUANTIFICATION AND STATISTICAL ANALYSIS

Statistical analyses were performed using Microsoft Office 365/Excel. Statistical details are given in the figure legends. Mean represents the average value of all samples, e.g., mean = [sum of sample values]/ [sample size]. Generally, plots show the mean ± standard deviation. Sample size (n) is given in the figure legends for each set. Significance levels are marked as * $p < 0.05$, as stated in the figure descriptions.

DATA AND CODE AVAILABILITY

The codes for implementing the model of lateral inhibition are uploaded to the following public URL: https://store.mbi.nus.edu.sg/tim/rhizoid_code.zip. This URL is hosted by the Mechanobiology Institute, the host institute for TES.